Journal of Power Sources 195 (2010) 2989–2995

Contents lists available at ScienceDirect

Journal of Power Sources

journal homepage: www.elsevier.com/locate/jpowsour

A novel approach to titania nanowire arrays as photoanodes of back-illuminated dye-sensitized solar cells

Ru-Hua Tao[b,c], Jin-Ming Wu[a,*], Hong-Xing Xue[a], Xiao-Mei Song[a], Xu Pan[c], Xia-Qin Fang[c], Xiao-Dong Fang[b,c], Song-Yuan Dai[c]

[a] Department of Materials Science and Engineering, Zhejiang University, Zheda Road 38#, Hangzhou 310027, Zhejiang, PR China
[b] Anhui Institute of Optics and Fine Mechanics, Chinese Academy of Sciences, Hefei 230031, PR China
[c] Key Lab of Novel Thin Film Solar Cells, Institute of Plasma Physics, Chinese Academy of Sciences, P. O. Box 1126, Hefei, Anhui 230031, PR China

ARTICLE INFO

Article history:
Received 15 September 2009
Received in revised form
15 November 2009
Accepted 18 November 2009
Available online 22 November 2009

Keywords:
Titanium dioxide
Dye-sensitized solar cell
Nanowire
Nanotube

ABSTRACT

Titania nanowire arrays have been deposited on Ti foils through direct oxidizing the Ti substrate with aqueous hydrogen peroxide solutions containing melamine and nitric acid, and the applicability of such nanowire arrays to back-illuminated dye-sensitized solar cells studied in parallel with titania nanotube arrays on Ti foils. The low-temperature nitrogen adsorption measurement reveals that the film with nanowires 25 nm in diameter and 1 μm in length possesses a BET specific surface area of 59.0 $m^2 g^{-1}$, a value much larger than 26 $m^2 g^{-1}$ calculated for the nanotube with an inner diameter of 80 nm, an outer diameter of 120 nm and a total length of 3 μm. Assuming an indirect transition between band gaps, the nanowire film exhibits a bandgap of 3.1 eV, slightly larger than that of 3.0 eV for the nanotube one. A detailed electrochemical study suggests that, in comparison with the nanotube film, the nanowire one exhibits much lower saturated photocurrent and poorer conductivity under the Xe-lamp irradiation. However, when utilized to construct back-side illuminated dye-sensitized solar cells, the cell with the 2 μm-thick nanowire photoanode possesses significantly higher efficiency than the one with the 3 μm-thick nanotube photoanode. The relatively high energy conversion efficiency is contributed to the high specific surface area and the unique mesoporous structure of the titania nanowire arrays, which favors the adsorption of dye molecules.

1. Introduction

With a maximum light-to-electricity conversion efficiency optimized to 11.0% in lab [1], dye-sensitized solar cells (DSSCs) have become the most promising alternative to the conventional silicon-based solar cells. In a widely adopted nanoparticulate titania (TiO_2)-based DSSC, the dye sensitizer adsorbs photons to excite electrons to be injected to the conduction band of titania, which then transport to a current collector to generate a photocurrent. The macroscopic assembly of the titania nanoparticles, which served as a photoanode, determines to a great extent the efficiency of a DSSC [2–4]. The mesoporosity and nanocrystallinity of the semiconductor are important for the adsorption of a large amount of dye molecules, for a thorough infiltration of electrolyte to titania nanoparticles for screening of injected electrons, and for the depletion of the nanoparticles upon immersion in the electrolyte to allow for a large photovoltage [5]. On the other hand, titania aggregates with unique nanofeatures, such as nanorods [6] and nanowires [7] are also found to contribute beneficially to the high efficiency due mainly to an improved electron transfer through the titania photoanode to the current collector. As compared with randomly distributed titania nanowires, the well-aligned titania nanowire arrays, especially the single-crystalline one, enhanced the charge collection and transport rate and in turn the light conversion efficiency [8,9]. Titania nanotube arrays deposited either on transparent conducting oxide (TCO)-coated glass substrates [10] or metallic Ti substrates [11] are also believed to be ideal candidates of photoanodes for high-efficiency DSSCs.

Titania thin films deposited on metallic foils are appropriate for constructing flexible, back-illuminated DSSCs [11]. There have appeared several techniques to fabricate titania nanowire arrays, in a crystal structure of either anatase or rutile, on Ti foils [12–16]; however, to explore a simple and easily scaled-up approach is still of interest to the low-cost fabrication of flexible DSSCs. In this paper, titania nanowire arrays were deposited on Ti foils by direct oxidizing the Ti substrate with aqueous hydrogen peroxide solutions containing certain amounts of melamine and nitric acid at a low temperature of 80 °C. The applicability of such nanowire arrays as photoanodes to DSSC was studied in comparison with titania

* Corresponding author. Tel.: +86 571 87953115; fax: +86 571 87952358.
E-mail address: msewjm@zju.edu.cn (J.-M. Wu).

0378-7753/$ – see front matter © 2009 Elsevier B.V. All rights reserved.
doi:10.1016/j.jpowsour.2009.11.075

nanotube arrays on Ti foils fabricated through an anodic oxidation approach.

2. Experimental details

2.1. Fabrication and characterization of titania nanowire and nanotube arrays

Titanium foils of the dimensions 5 cm × 5 cm × 0.01 cm were pickled in a 1:3:6 (in volume) mixture of a 55 mass% HF aqueous solution, a 63 mass% HNO_3 aqueous solution and distilled water, for 2 min, followed by cleaning in an ultrasonic bath. To fabricate titania nanowire arrays, each Ti foil was immersed in 50 ml 30 mass% H_2O_2 solution which contained 15 mg melamine ($C_3H_6N_6$) and 1.0 ml 63 mass% HNO_3, and kept in an oven maintained at 80 °C for 72 h [16]. The surface-oxidized Ti was then rinsed in distilled water, dried at 80 °C, and subjected to a thermal treatment at 450 °C for 1 h in air.

Titania nanotube arrays were fabricated with a technique slightly modified based on the literature [17]. The pickled Ti foil was oxidized in a mixture of glycol and water (98:2 in volume) containing NH_4F (0.3 mass%) by using a two-electrode configuration with a platinum foil as a counter electrode, under a constant anodic potential of 50 V for 1.5 h at room temperature. The film was subjected to a final thermal treatment at 500 °C for 2 h in air.

The produced thin films were characterized by X-ray diffraction (XRD, Rigaku D/max-3B diffractometer, Tokyo, Japan) with Cu Kα radiation operated at 40 kV, 36 mA (λ = 0.154056 nm), field emission scanning electron microscopy (FE-SEM, Sirion-100, FEI, Eindhoven, the Netherlands), and UV–vis near-infrared spectrometer (UV-3150, Shimadzu, Tokyo, Japan). The nitrogen sorption measurement was conducted at 77 K using Autosorb-1 (Quantachrome Instruments). All the electrochemical experiments were performed in a standard three-electrode configuration with a platinum plate as counter electrode and a saturated calomel electrode (SCE) as reference electrode using an electrochemical working station (CHI-660C, Shanghai Chenhua, China). A 0.25 M Na_2SO_4 solution (pH = 6.3) was used as supporting electrolyte, the pH value of which being not controlled during the reaction. The specimens were sealed with epoxy to expose an active area of 1.0 cm × 1.0 cm. When necessary, a 500 W Xe-lamp was used to provide the light illumination, the intensity of which reaching the specimen was measured to be ca. 5.0 mW cm^{-2} and 200.0 mW cm^{-2}, respectively, for the UV and visible irradiance using irradiance meters (Model: UV-A and FZ-A, Beijing Normal University, China, measured for the wavelength range of 320–400 nm with a peak wavelength of 365 nm for UV light, and 400–1000 nm for visible light). The electrochemical impedance spectra (EIS) were obtained at the open-circuit potential of the specimen, with an amplitude of 5 mV. The frequency span was from 100 kHz down to 0.01 Hz. The measured EIS spectra were fitted using the ZSimpWin software (Version 3.10, by Echem).

2.2. Assembly and characterization of the solar cell

The titania films on Ti substrates with sizes of 1.0 cm × 1.0 cm were immersed in a 0.5 mM *cis*-di(thiocyanate)-bis(2,2′-bipyridyl-4,4′-dicarboxylate)-ruthenium (II) bis-tetrabutlammonium (N719) in anhydrous ethanol solution overnight. The excess of N719 dye in the titania film was rinsed off with anhydrous ethanol before assembly. The attenuated total reflection Fourier transform infrared (ATR FTIR) spectra of dye-sensitized titania films were recorded using MAGNA-IR 750 (Nicolet Instrument Co. Ltd., USA). The counter electrode was platinized by spraying H_2PtCl_6 solution to a TCO-coated glass and fired in air at 410 °C for 20 min, which was then placed directly on the top of the dye-sensitized titania film. The gap between the two electrodes was sealed by thermal adhesive films (Surlyn, Dupont). The electrolyte, which consisted of 0.1 M LiI, 0.6 M 1,2-dimethyl-3-*n*-propylimidazolium iodide (DMPII), 0.5 M I_2, and 1 M 4-tert-butylpyridine (TBP) in methoxyacetonitrile, was

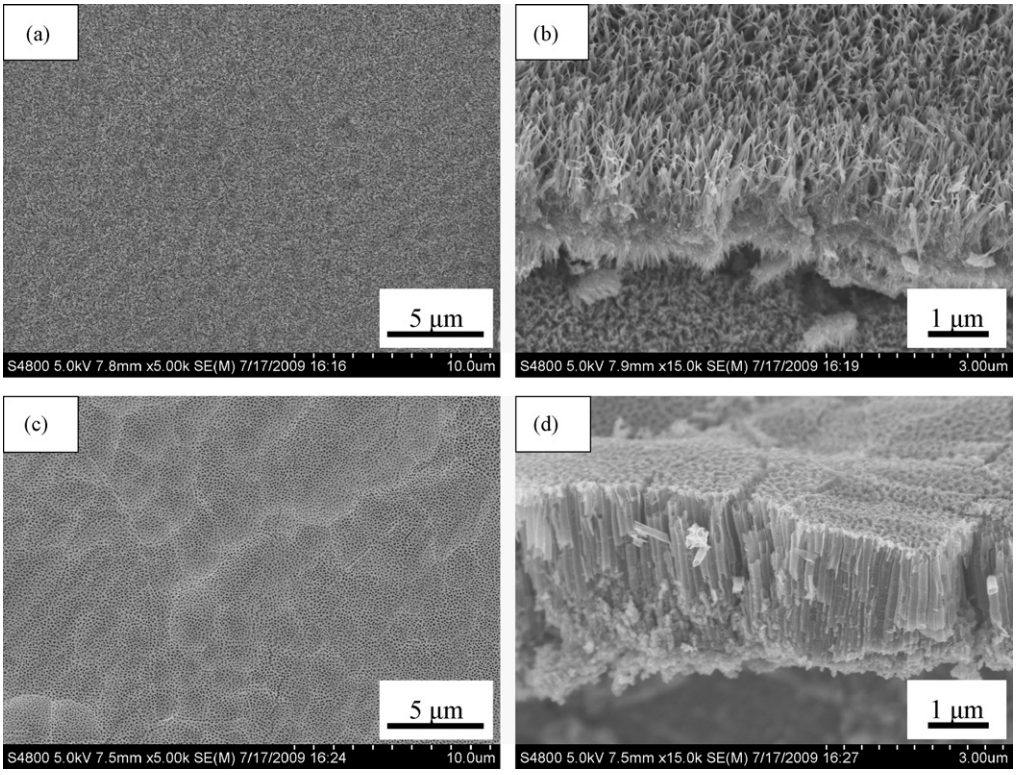

Fig. 1. FE-SEM images of titania (a and b) nanowire and (c and d) nanotube arrays.

filled from a hole made on the counter electrode, which was later sealed by a cover glass and thermal adhesive films. The total active electrode area of DSSCs was 0.25 cm^2. The photovoltaic performance of DSSCs was measured with a Keithley 2400 source meter controlled by Testpoint software under solar simulator (Xenon lamp, AM1.5, 100 mW cm^{-2}, Changchun Institute of Optics Fine Mechanics and Physics, Chinese Academy of Sciences, calibrated with standard crystalline silicon solar cell).

For comparison, anatase colloidal solution was prepared by hydrolysis of titanium tetraisopropoxide according to the literature [18]. The BET specific surface area of the powder was 80 $m^2 g^{-1}$ and the average particle size was 13.6 nm. The titania paste was deposited on the pickled Ti foil by using a doctor-blade technique, and sintered in air at 450 °C for 30 min to form the nanoparticulate titania electrode with a film thickness of 4.5 μm.

3. Results and discussion

Fig. 1 shows FE-SEM morphologies of the titania nanowire and nanotube arrays deposited on the Ti foil. Homogeneous titania nanowire and nanotube arrays have been fabricated successfully, as can be discerned from the low-magnification images shown in Fig. 1a and c, respectively. The cross-sectional image illustrated in Fig. 1b revealed that the nanowire was ca. 25 nm in diameter and

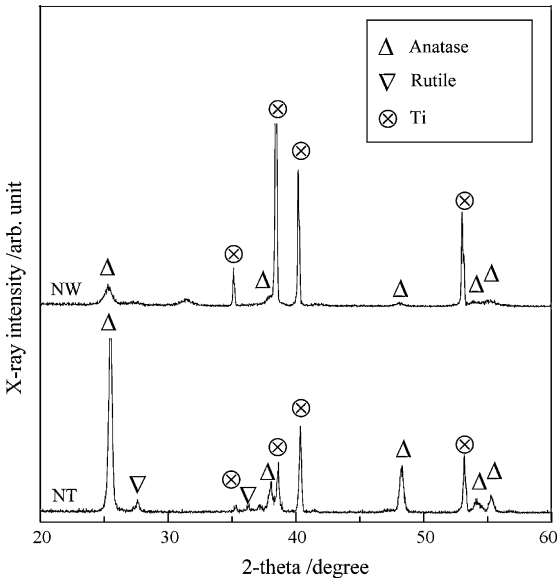

Fig. 2. XRD patterns of titania nanowire (NW) and nanotube (NT) arrays.

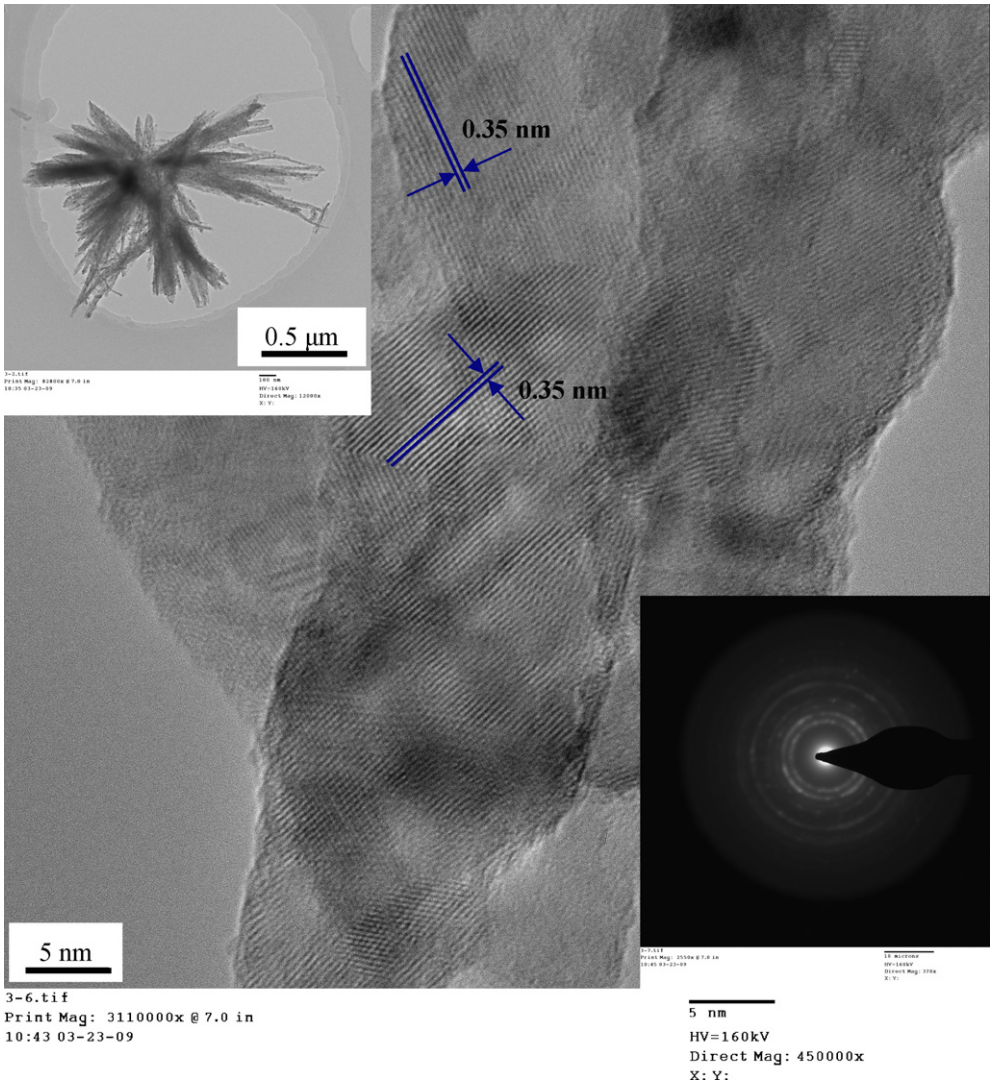

Fig. 3. HR-TEM image of the titania nanowire. A low-magnification image and the corresponding selected-area electron diffraction pattern are demonstrated as insets.

1 μm in length, with an intermediate compact layer of ca. 1 μm. The nanotube possessed an inner diameter of ca. 80 nm, an outer diameter of ca. 120 nm and a total length of ca. 3 μm (Fig. 1d). The nanowires separated from each other, providing numerous open channels for the dyes and electrolytes to reach and surround the whole wire when utilized as photoanodes for DSSCs. For the nanotube, such channels were provided predominantly by the tube itself as neighboring tubes came to intimate contact with each other.

Fig. 2 illustrates the XRD patterns for the nanowire and nanotube arrays after the calcination to achieve a full crystallization. Both films consisted predominantly of anatase; however, trace rutile can be identified for the nanotube arrays. The nanotube array possessed significantly stronger intensity for the peaks corresponding to anatase, which can be attributed to the thicker film. A rough estimation of the grain size utilizing the Scherrer's formula [19] gave a value of ca. 12.3 nm for the nanowire and 26.1 nm for the nanotube, respectively.

Similar to the nanotube walls, the nanowire consisted also of polycrystalline anatase. Fig. 3 indicates the HR-TEM image of a nanowire with distinct grains 10–15 nm in size. Several regions of parallel fringes with a distance of 0.35 nm between the two adjacent one, which corresponds to the interplaner distance of anatase {1 0 1} can be discerned. The selected-area diffraction pattern (the inset in Fig. 3) is in good agreement with the XRD pattern (Fig. 2).

Titania nanowires were scratched off the corresponding films and subjected to the nitrogen adsorption–desorption measurement under a low temperature of 77 K. As shown in Fig. 4a, the obtained curve exhibited a type IV nitrogen isotherm with a type H3 desorption hysteresis loop, which suggests the existence of mesopores [20]. The Brunauer–Emmett–Teller (BET) specific surface area determined using the adsorption data with a relative pressure range below 0.30 was 59.0 $m^2\,g^{-1}$, which almost doubled the calculated specific surface area of ca. 26 $m^2\,g^{-1}$ for the array consisted of nanotubes with an inner diameter of 80 nm and a wall thickness of 20 nm [21]. Fig. 4b shows the pore size distribution curve estimated by the Barrett–Joyner–Halenda (BJH) method, which gave a mean pore size of 19.4 nm and a total pore volume of 0.24 $cm^3\,g^{-1}$.

Fig. 5a demonstrates the UV–vis diffuse reflectance spectra collected from the nanowire and nanotube arrays on Ti substrates. The nanowire arrays exhibited lower reflectance over both the UV and the visible light regions, which suggests a much higher capability for the nanowire arrays to absorb light when compared with the nanotube arrays. Assuming an indirect transition between band gaps, the bandgap of titania can be estimated by extrapolating the tangent line in the plot of $\alpha^{1/2}$ against $h\nu$, where, α is the absorption coefficient and $h\nu$ is the photon energy. Fig. 5b demonstrates that the nanowire arrays possessed an indirect bandgap of 3.12 eV, which is larger than the value of 3.00 eV determined for the nanotube arrays. Bulk titania possessed a bandgap of 3.2 eV for anatase and 3.0 eV for rutile [22]. The slightly red-shift for the nanowire arrays was attributed mainly to the large amounts of surface oxygen-deficiencies due to the remarkable incorporation of hydroxyl groups [16]. The XRD pattern revealed trace rutile in the nanotube arrays; therefore, an even narrower bandgap was measured. Possible incorporation of carbon in the titania nanotube, which resulted from the organic electrolyte during the anodic oxidation, contributed also to the red-shift in the responsive light.

Fig. 6 demonstrates the current–voltage curve of the nanowire and nanotube arrays both in the dark and under the Xe-lamp irradiation. Both electrodes exhibited neglectable anodic current in the dark with the bias potential up to 1.0 V vs. SCE. Under the light illumination, a saturated photocurrent of 0.90 mA cm^{-2} and 0.12 mA cm^{-2}, respectively, was detected for the nanotube and nanowire arrays. The remarkable higher photocurrent for the nanotube arrays can be attributed partly to the thicker film (Fig. 1), longer responsive light wavelength (Fig. 5) and higher film conductivity as will be revealed by the EIS measurement.

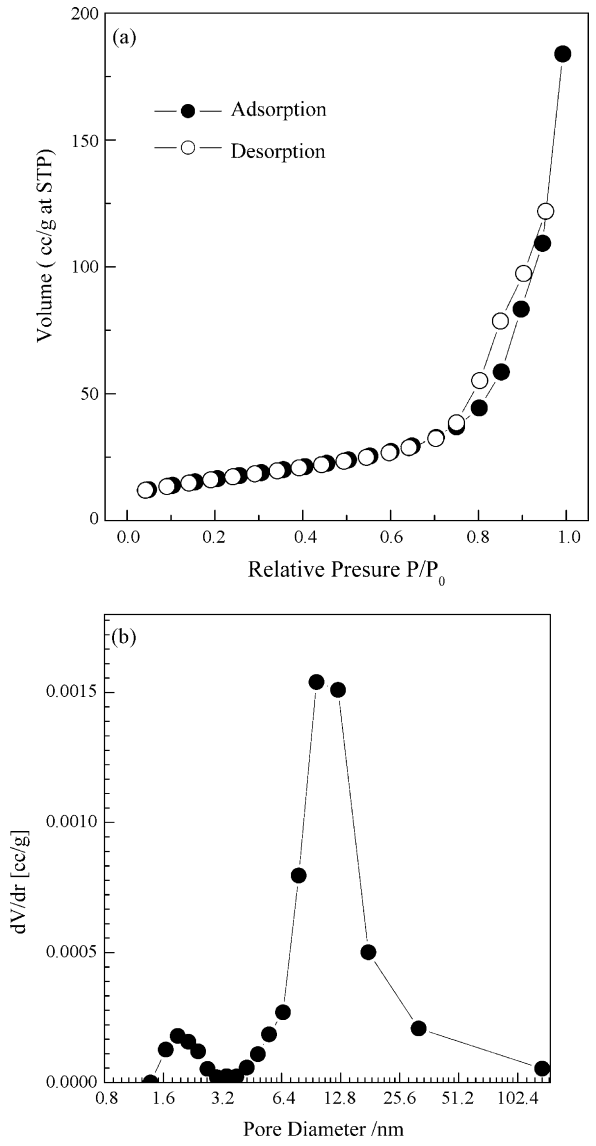

Fig. 4. Nitrogen adsorption–desorption isotherm (a) and the pore size distribution curve as determined using desorption data and the BJH model (b) for powders scratched off the titania nanowire film on Ti substrates.

Fig. 7 shows the measured and calibrated Nyquist plots of the nanowire and nanotube electrodes under the Xe-lamp irradiation. The following circuit was found to give the best fitting result for the two thin film electrodes,

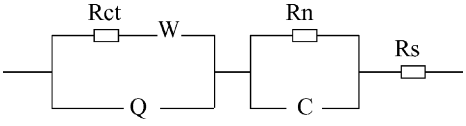

where, Q represents the double-layer capacitance on the electrode, R_{ct} is the apparent resistance and W represents the Warburg impedance due to mass transfer from the bulk of the electrolyte to the reaction site, R_n and C in parallel combination represent cations/anions extruded into the titania film to maintain an electroneutrality, and R_s simulates both the solution resistance and the uncompensated potential drop. Table 1 lists the extracted parameters for the circuit elements evaluated by fitting the impedance

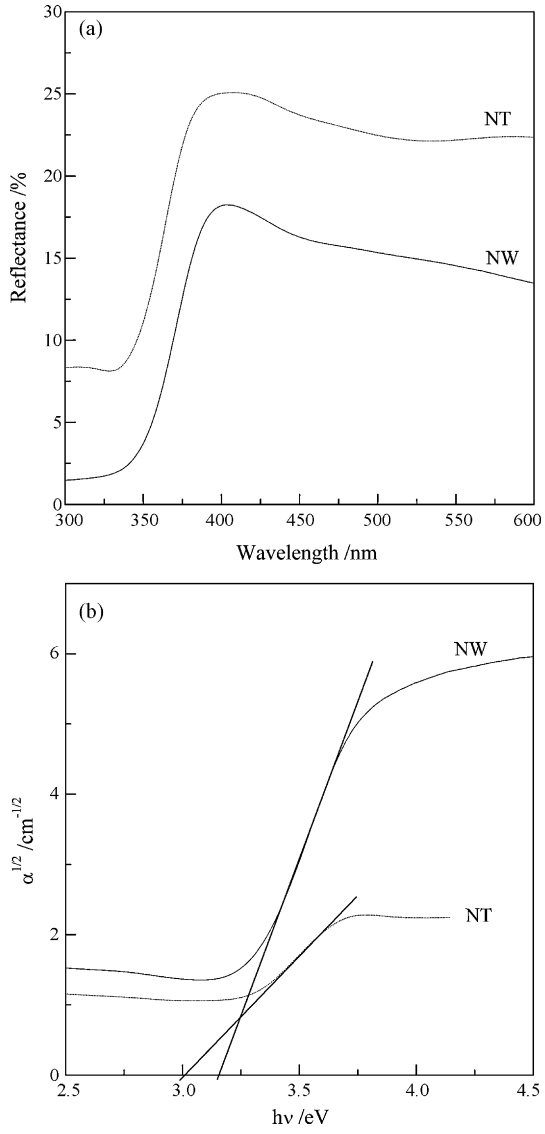

Fig. 5. (a) UV–vis diffuse reflectance spectra of titania nanowire (NW) and nanotube (NT) arrays. (b) Re-plotting of (a) in the $\alpha^{1/2} \sim h\nu$ coordinate to evaluate the corresponding band gap, assuming an indirect transition between bands for titania.

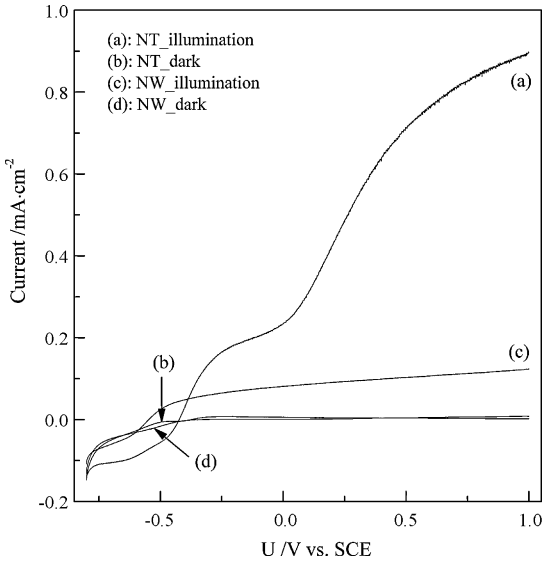

Fig. 6. Current vs. potential diagrams of thin film electrodes consisted of titania nanowire (NW) and nanotube (NT) arrays in the dark and under illumination.

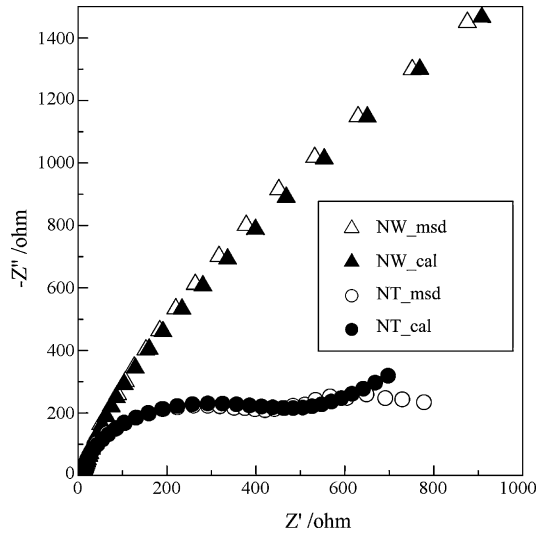

Fig. 7. Measured and calibrated Nyquist diagrams of titania nanowire (NW) and nanotube (NT) arrays under illumination.

data. The value of R_s kept almost constant for the two cases. The nanotube electrode exhibited significantly larger double-layer capacitance than that of the nanowire one; yet the latter possessed a value of R_{ct} one order larger. The reciprocal of the product of R_{ct} and Q gave a parameter K_{eff} that defining the recombination rate constant of the overall photoelectrochemical reaction [23],

$$K_{eff} = \frac{1}{R_{ct} \times Q} \quad (1)$$

Table 1 illustrates that, the K_{eff} value for the nanowire array was significantly larger than that for the nanotube array. The smaller overall recombination rate constant for the nanotube arrays contributed also to the higher saturated photocurrent (Fig. 6).

Under AM 1.5 illumination, *I–V* characteristics of the DSSCs constructed utilizing the titania nanowire and nanotube arrays as photoanodes are illustrated in Fig. 8. Table 2 indicates the derived short-circuit photocurrent (J_{sc}), open-circuit voltage (V_{oc}), fill factor (FF) and the cell efficiency. For comparison, a DSSC with photoanode of a 4.5 μm-thick film deposited on the pickled Ti foil by anatase nanoparticles through a doctor-blade approach was also included. The anatase nanoparticles-based DSSC exhibited a J_{sc} of

Table 1
Selected parameters for the circuit elements evaluated by fitting the impedance data to the equivalent circuits for the titania nanowire (NW) and nanotube (NT) electrodes in 0.25 M Na_2SO_4 with the Xe-lamp irradiation.

Electrodes	Equivalent circuits	Parameters by fitting				
		R_s (Ω cm²)	Q (μF cm⁻²)	R_{ct} (Ω cm²)	R_n (Ω cm²)	K_{eff} (s⁻¹)
NW	$R_s(Q(R_{ct}W)CR_n)$	8.4 (1.0%)	30.8 (2.4%)	7476 (1.2%)	156.0 (16.2%)	4.35
NT	$R_s(Q(R_{ct}W)CR_n)$	8.2 (0.8%)	968.3 (1.6%)	441.1 (1.9%)	1.0 (8.9%)	2.34

The numbers in the parentheses are the estimated errors.

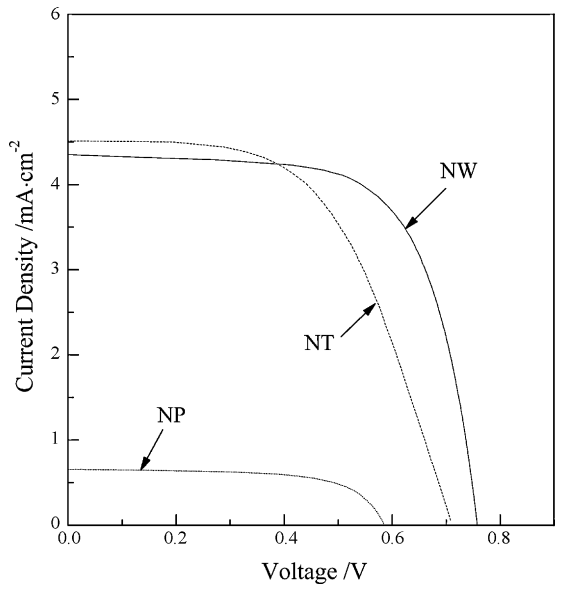

Fig. 8. Current–voltage curves of DSSCs constructed with photoanodes of titania nanowire (NW), nanotube (NT) arrays and commercial nanoparticles (NP).

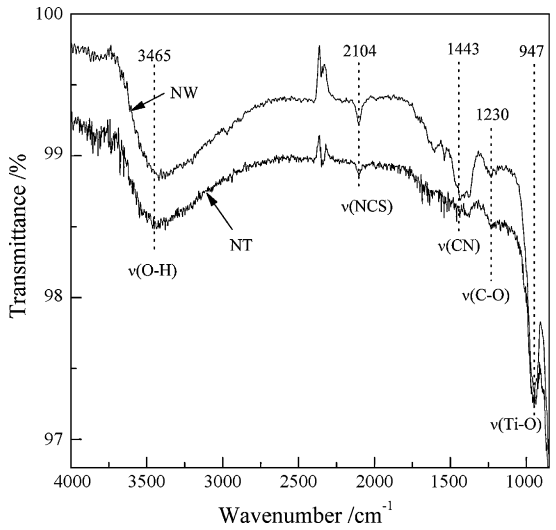

Fig. 9. ATR FTIR spectra of titania nanowire (NW) and nanotube (NT) arrays.

0.65 mA cm^{-2}, a V_{oc} value of 0.59 V and a FF of 0.66 to produce an overall conversion efficiency of only 0.253%. Because the anatase nanoparticles utilized to fabricate the photoanode possessed a high specific surface area of 80 m^2 g^{-1}, the poor performance of the DSSC was attributed mainly to the easily occurred recombination of injected electrons with I_3^- (dark current) on the Ti substrate because of the failure of a full coverage of the pickled Ti with anatase nanoparticles.

The cell NT (see Table 2 also for the notation) exhibited a J_{sc} of 4.50 mA cm^{-2}, a V_{oc} value of 0.72 V and a FF of 0.55 to produce an overall conversion efficiency of 1.78%. The FF of only 0.55 was significantly lower than the other two cells. Mor et al. constructed a DSSC utilizing highly ordered titania nanotube arrays, with a thickness of 360 nm, on FTO substrates and achieved a fill factor of 0.49, which, they attributed to the large series resistance as a result of the barrier layer and poor contact between the barrier layer and FTO substrate [10]. When titania nanotube arrays grown directly on the Ti substrates (6 μm long) were utilized to construct a back-illuminated DSSC, Paulose et al. achieved a high FF of 0.57 [11], a value near to the present work, because of the absence of the resistance arising from the interface between the barrier layer and the FTO or ITO substrate. The overall conversion efficiency of the back-illuminated DSSC constructed by Paulose et al., infiltrated with N-719 in acetonitrile, was 4.24% [11], much higher than the cell NT in our work; however, the present efficiency of 1.78% for the cell NT is reasonable because Paulose et al. utilized the nanotube arrays with doubled length and performed a $TiCl_4$-treatment to the nanotube arrays, which improved further the DSSC efficiency. In addition, it is noted that, using ethanol to infiltrate the N719, as the case in the current investigation, resulted in a decrease of short-circuit current density and open-circuit voltage by about 35% [11].

Compared with the nanoparticulate-based DSSC, the two cells based on titania nanowire and nanotube arrays exhibited significantly higher efficiency. The cell efficiency was expected to increase with increasing film thickness of the photoanodes for cells NW (2.0 μm), NT (3.0 μm) and NP (4.5 μm); yet the cell NP exhibited the lowest J_{sc}, V_{oc} and in turn cell efficiency, which evidenced the beneficial effects of photoanodes with ordered nanostructures. High-efficient creation of photon-excited electrons and their effective transport to the collective electrode are the keys to a solar cell with high performances. Photoanodes with ordered nanostructures such as nanowires and nanotubes are believed to inhibit the recombination of electron–hole pairs and favor the migration of the photogenerated electrons.

The cell NW possessed slightly lower short-circuit photocurrent, but higher open-circuit voltage and significantly higher fill factor than the cell NT. The thickness of the photoanodes for the cell NW and NT was ca. 2.0 and 3.0 μm, respectively. In addition, the photoelectrochemical characterizations suggested significantly higher photocurrent and lower recombination rate constant of the nanotube arrays when compared to the nanowire arrays. Therefore, the fact that the cell NW exhibited a short-circuit photocurrent only slightly lower than that of the cell NT can be explained only by the amounts of the adsorbed N719 dye molecules. Fig. 9 indicates the ATR FTIR spectra of the two photoanodes after adsorption of the N719 dye. The peak located at 947 cm^{-1} originated from titania and the broad one located at around 3465 cm^{-1} resulted from the adsorbed water. The three peaks located at 1230, 1443 and 2104 cm^{-1} correspond to the C–O, –CN and –NCS groups as a result of N719 adsorption [24]. The intensity of the peak corresponding to the vibration of –NCS was remarkably stronger on the nanowire array when compared with that on the nanotube array, suggesting more dye molecules adsorbed on the nanowire arrays, which contributes to the photocurrent achieved for the cell NW. The higher capability of titania nanowire arrays to adsorb dyes can be ascribed to the higher surface area over the nanotube arrays. The mesopores with an average diameter of 19.4 nm and a total pore volume of 0.24 cm^3 g^{-1} were believed to contribute additionally to the dye adsorption. In addition, the present titania nanowires

Table 2
Performance characteristics of the dye-sensitized solar cells constructed with the various photoelectrodes.

Cell notation	Photoanode	V_{oc} (V)	J_{sc} (mA cm^{-2})	FF (%)	η (%)
NP	4.5 μm-thick nanoparticulate film	0.59	0.65	66	0.253
NT	3.0 μm-thick nanotube film	0.72	4.50	55	1.78
NW	2.0 μm-thick nanowire film	0.76	4.35	67	2.22

exposed mainly anatase {1 0 1} facets (Fig. 3), which are reported to favor the adsorption of the N719 dye [7,25].

The unique porous top morphology for the titania nanowire array as shown in Fig. 1 was believed also to favor the full infiltration of electrolytes when compared with the nanotubes, which helped to the charge separation. Furthermore, the relatively efficient light-harvesting of the nanowire arrays, as revealed by the UV–vis diffuse reflectance spectra (Fig. 5) benefited also the high light-to-electricity efficiency for the cell NW. It is argued that the light can be absorbed along the long axis of the wire/rod and the charge carriers can diffuse a short distance radially to the wire/electrolyte interface [26].

The relatively high FF of 0.67 for the cell NW, which is comparable to that of the cell NP, contributed predominantly to its high efficiency over the cell NT. The FE-SEM observation demonstrated that the titania nanowire array fabricated in the present work exhibited a barrier layer with a thickness of ca. 1 μm, which was much thicker than that of the nanotube array (Fig. 1). The EIS spectra analysis gave a much lower conductivity of the nanowire arrays than that of the nanotube film. However, the series resistance of the cell NW, which can be estimated from the inverse slope in the linear region of the *I–V* curve near the V_{oc}, decreased to 42% of that of the cell NT [8], which explained the high FF of the cell NW. As a preliminary explanation, the high FF might be a result of the relatively high V_{oc} [27], which resulted from the wider indirect bandgap of the nanowire array over the nanotube one because a higher position of the conduction band of titania contributes to a high V_{oc} of DSSCs [28].

4. Conclusion

Titania nanowire arrays consisted mainly of anatase were deposited on Ti foils through a simple solution approach followed by calcination. The calcinated nanowires possessed a high specific surface area of 59 $m^2\ g^{-1}$, exhibiting mesopores with an average diameter of 19.4 nm and a total pore volume of 0.24 $cm^3\ g^{-1}$. Electrochemical characterizations revealed that, in comparison with the 3 μm-thick nanotube film fabricated by anodic oxidation of Ti foils, the 2 μm-thick nanowire film exhibited lower saturated photocurrent as well as poorer conductivity under the Xe-lamp irradiation. However, the back-illuminated N719 dye-sensitized solar cell constructed with the nanowire array possessed a short-circuit photocurrent of 4.35 mA cm^{-2}, an open-circuit voltage of 0.76 V vs. SCE and a fill factor of 0.67 with an overall cell efficiency of 2.22%, in comparison with the corresponding values of 4.50 mA cm^{-2}, 0.72 V, 0.55 and 1.78% for the one constructed with the nanotube arrays. The superior performance of the titania nanowire arrays over the nanotube one was contributed to the more N719 dye molecules adsorbed on the nanowire array because of the high specific surface area and the unique mesoporous characteristics. As a result, the present study provides a possible approach to low-cost large-scale fabrication of photoanodes for flexible back-illuminated dye-sensitized solar cells with high efficiency.

Acknowledgements

This work is supported by Zhejiang Provincial Natural Science Foundation of China (Grant No. Y408001) and Anhui Provincial Natural Science Foundation of China (Grant No. 090414169).

References

[1] J.H. Yum, P. Chen, M. Gratzel, M.K. Nazeeruddin, ChemSusChem 1 (2008) 699–707.
[2] J. Bisquert, A. Zaban, P. Salvador, J. Phys. Chem. B 106 (2002) 8774–8782.
[3] L.Y. Liang, S.Y. Dai, L.H. Hu, F.T. Kong, W.W. Xu, K.J. Wang, J. Phys. Chem. B 110 (2006) 12404–12409.
[4] X. Pan, S.Y. Dai, K.J. Wang, L.H. Hu, C.W. Shi, L. Guo, F.T. Kong, Chin. J. Chem. 23 (2005) 1579–1583.
[5] D. Cahen, G. Hodes, M. Gratzel, J.F. Guillemoles, I. Riess, J. Phys. Chem. B 104 (2000) 2053–2059.
[6] J.T. Jiu, S. Isoda, F.M. Wang, M. Adachi, J. Phys. Chem. B 110 (2006) 2087–2092.
[7] M. Adachi, Y. Murata, J. Takao, J.T. Jiu, M. Sakamoto, F.M. Wang, J. Am. Chem. Soc. 126 (2004) 14943–14949.
[8] H.S. Shim, S.I. Na, S.H. Nam, H.J. Ahn, H.J. Kim, D.Y. Kim, W.B. Kim, Appl. Phys. Lett. 92 (2008) 183107.
[9] X. Feng, K. Shankar, O.K. Varghese, M. Paulose, T.J. Latempa, C.A. Grimes, Nano Lett. 8 (2008) 3781–3786.
[10] G.K. Mor, K. Shankar, M. Paulose, O.K. Varghese, C.A. Grimes, Nano Lett. 6 (2005) 215–218.
[11] M. Paulose, K. Shankar, O.K. Varghese, G.K. Mor, B. Hardin, C.A. Grimes, Nanotechnology 17 (2006) 1446–1448.
[12] B. Liu, J.E. Boercker, E.S. Aydil, Nanotechnology 19 (2008) 505604.
[13] J.J. Wu, C.C. Yu, J. Phys. Chem. B 108 (2004) 3377–3379.
[14] J.M. Wu, J. Cryst. Growth 269 (2004) 347–355.
[15] S. Daothong, N. Songmee, S. Thongtem, P. Singjai, Scr. Mater. 57 (2007) 567–570.
[16] J.M. Wu, H.X. Xue, J. Am. Ceram. Soc. 92 (2009) 2139–2143.
[17] J.M. Macak, P. Schmuki, Electrochim. Acta 52 (2006) 1258–1264.
[18] C.W. Shi, S.Y. Dai, K.J. Wang, X. Pan, L.Y. Zeng, L.H. Hu, F.T. Kong, L. Guo, Electrochim. Acta 50 (2005) 2597–2602.
[19] J.M. Wu, S. Hayakawa, K. Tsuru, A. Osaka, J. Am. Ceram. Soc. 87 (2004) 1635–1642.
[20] J.M. Wu, Environ. Sci. Technol. 41 (2007) 1723–1728.
[21] O.K. Varghese, D.W. Gong, M. Paulose, K.G. Ong, E.C. Dickey, C.A. Grimes, Adv. Mater. 15 (2003) 624–627.
[22] J.M. Wu, M. Antonietti, S. Gross, M. Bauer, B.M. Smarsly, ChemPhysChem 9 (2008) 748–757.
[23] M. Adachi, M. Sakamoto, J.T. Jiu, Y. Ogata, S. Isoda, J. Phys. Chem. B 110 (2006) 13872–13880.
[24] A.I. Philippopoulos, A. Terzis, C.P. Raptopoulou, V.J. Catalano, P. Falaras, Eur. Inorg. Chem. (2007) 5633–5644.
[25] V. Shklover, Y. Ovchinnikov, L.S. Braginsky, S.M. Zakeeruddin, M. Gratzel, Chem. Mater. 10 (1998) 2533–2541.
[26] P.V. Kamat, J. Phys. Chem. C 112 (2008) 18737–18753.
[27] J.L. Gray, in: A. Luque, S. Hegedus (Eds.), Handbook of Photovoltaic Science and Engineering, John Wiley & Sons, Inc., NJ, 2003, pp. 61–112.
[28] Q. Wang, S. Ito, M. Gratzel, F. Fabregat-Santiago, I. Mora-Sero, J. Bisquert, T. Bessho, H. Imai, J. Phys. Chem. B 110 (2006) 25210–25221.